Accuracy and Stability of Virtual Source Method for Numerical Simulations of Nonlinear Water Waves

Omar Al-Tameemi [a], *David I. Graham* [a], *and Kurt Langfeld* [b]
[a] School of Computing, Electronics and Mathematics, Plymouth University, UK
[b] Department of Mathematical Sciences, University of Liverpool, UK

ABSTRACT

The virtual source method (VSM) developed by Langfeld et al., (2016) is based upon the integral equations derived by using Green's identity with Laplace's equation for the velocity potential. These authors presented preliminary results using the method to simulate standing waves. In this paper, we numerically model a non-linear standing wave by using the VSM to illustrate the energy and volume conservation. Analytical formulas are derived to compute the volume and potential energy while the kinetic energy is computed by numerical integration. Results are compared with both theory and boundary element method (BEM).

KEY WORDS: Numerical wave tank (NWT), boundary integral equation, energy conservation, accuracy, stability.

INTRODUCTION

Many methods have been developed to study wave/structure interactions numerically by using the so called numerical wave tank (NWT). A comprehensive approach is to use 'CFD' methods to solve the full Navier-Stokes equations. For example Huang et al. (1998) developed a numerical model to simulate a nonlinear wave fields generated by a piston-type wavemaker by solving Navier-Stokes equations. Park et al (2001) developed the viscous 3D numerical wave tank to simulate regular, irregular and fully nonlinear multi-directional waves. However, a simple but common approach is the use of the fluid potential. Longuet-Higgins and Cokelet (1976) simulated an overturning wave using potential flow theory with a mixed Eulerian-Lagrangian method in combination with a boundary integral equation formulation. Wu and Taylor (1994) employed the finite element method for the nonlinear potential flow equation. Grilli et al. (2001) introduced the development of three-dimensional numerical wave tanks which contains an arbitrary bottom topography, sloping beach and the possibility to include wave makers. The nonlinear potential flow equation is solved with a combination of a boundary element method (BEM) and a mixed Eulerian-Lagrangian technique to compute the free surface motion. Recently, Langfeld et al. (2016) introduced the virtual source method (VSM) for solving free-surface potential flow problems and applied it to simulate standing waves in 2D and 3D.

In this paper we investigate the global error behaviour of the VSM for standing waves. The results are compared with the boundary element method solutions.

GOVERNING EQUATIONS AND TANK GEOMETRY

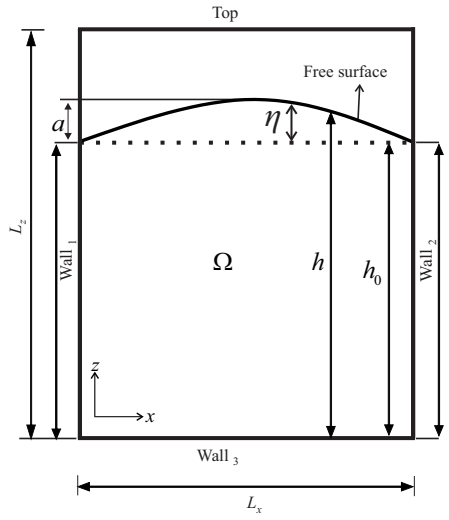

Fig. 1 Wave tank geometry.

An ideal fluid is assumed so that the fluid velocity can be described by the gradient of velocity potential ϕ. A Cartesian coordinate system is chosen such that z = 0 corresponds to the calm water level and z is positive upwards as shown in figure 1. Then the governing equation of the velocity potential in the fluid domain Ω is Laplace's equation,

$$\nabla^2\phi = \frac{\partial^2\phi}{\partial x^2} + \frac{\partial^2\phi}{\partial z^2} = 0. \tag{1}$$

On the free surface, the kinematic free surface boundary condition is defined as,

$$\frac{\partial \eta}{\partial t} = \frac{\partial \phi}{\partial z} + \frac{\partial \phi}{\partial x}\frac{\partial \eta}{\partial x} \qquad \text{on } z = \eta. \tag{2}$$

while the dynamic boundary condition is defined by the following equation.

$$\frac{\partial \phi}{\partial t} = -g\eta - \frac{1}{2}|\nabla\phi|^2 \qquad \text{on } z = \eta. \tag{3}$$

To satisfy the impermeability condition (no-flux condition), the normal velocity is set to be zero at the walls.

$$\frac{\partial \phi}{\partial n} = 0 \qquad \text{on Wall}_1\text{, Wall}_2 \text{ and Wall}_3. \tag{4}$$

BOUNDARY ELEMENT METHOD (BEM)

The boundary element method solves Laplace's equation (1) first by converting to a boundary integral equation and then dividing the problem boundary into small boundary elements. It results in a system of linear algebraic equations. In this paper, boundary element discretisation was done by using linear elements with piecewise constant variables.

Boundary Integral Equation

The velocity potential and the corresponding free surface profiles are obtained by solving the discretised form of the following integral equation:

$$\lambda(\mathbf{x}_0)\phi(\mathbf{x}_0) = \int_\Gamma \left(\phi(\mathbf{x})\frac{\partial G(\mathbf{x};\mathbf{x}_0)}{\partial n} - G(\mathbf{x};\mathbf{x}_0)\frac{\partial \phi(\mathbf{x})}{\partial n}\right) d\Gamma(\mathbf{x}), \tag{5}$$

where $\mathbf{x}$ and $\mathbf{x}_0$ are the source and field points, respectively, $G(\mathbf{x};\mathbf{x}_0)$ is the Green function satisfying Laplace equation, Γ is the boundary, and $\lambda(\mathbf{x}_0)$ is the collision angle at a point on the boundary.

Numerical Implantation of BEM

For a simple approximation of ϕ and $\frac{\partial \phi}{\partial n}$ on the boundary Γ, assume that these functions are constant over each of the boundary elements. Specifically, consider the approximation:

$$\begin{matrix} \phi \approx \bar{\phi}_k \\ \frac{\partial \phi}{\partial n} \approx \bar{p}_k \end{matrix} \;,\; \mathbf{x} \in \Gamma_k,\ (k = 1, 2, 3, ..., N), \tag{6}$$

where N is the number of boundary elements, $\bar{\phi}_k$ and $\bar{p}_k$ are the values of ϕ and $\frac{\partial \phi}{\partial n}$ at the midpoint of Γ_k respectively.
An approximation of (5) together with (6) can be written as:

$$\lambda(\mathbf{x}_0)\phi(\mathbf{x}_0) = \sum_{k=1}^{N} \{\bar{\phi}\, F_{2k}(\mathbf{x}_0) - \bar{p}_k F_{1k}(\mathbf{x}_0)\}, \tag{7}$$

where

$$F_{1k}(\mathbf{x}_0) = \int_{\Gamma_k} G(\mathbf{x};\mathbf{x}_0) ds(\mathbf{x}),$$

$$F_{2k}(\mathbf{x}_0) = \int_{\Gamma_k} \frac{\partial G(\mathbf{x};\mathbf{x}_0)}{\partial n} ds(\mathbf{x}). \tag{8}$$

To solve equation (7), we note that either $\bar{\phi}_k$ or $\bar{p}_k$ is known from (2)-(4). There are, therefore, N unknown constants on the right hand side of equation (7) to be computed by generating N equations include the unknowns. Consider that $(\mathbf{x}_0)$ in equation (7) is given at the midpoints of Γ_1, Γ_1, Γ_3, ..., Γ_N, then by using equation (5):

$$\frac{1}{2}\bar{\phi}_m = \sum_{k=1}^{k} \{\bar{\phi}_k F_{2k}(\bar{\mathbf{x}}_m) - \bar{p}_k F_{1k}(\bar{\mathbf{x}}_m)\},\ m = 1, 2, ..., N, \tag{9}$$

where $(\bar{\mathbf{x}}_m)$ is the midpoint of Γ_m.

Equation (9) forms a linear algebraic system of N equations containing the N unknowns on the right hand side of equation (7) and can be written as:

$$\sum_{k=1}^{N} a^{(mk)} z^{(k)} = \sum_{k=1}^{N} b^{(mk)},\ m = 1, 2, ..., N, \tag{10}$$

where $a^{(mk)}$, $b^{(mk)}$ and $z^{(k)}$ are defined as:

$$\begin{aligned}
a^{(mk)} &= \begin{cases} -F_{1k}(\bar{\mathbf{x}}_m), & \text{if } \phi \text{ is specified over } \Gamma_k \\ F_{2k}(\bar{\mathbf{x}}_m), & \text{if } \frac{\partial \phi}{\partial n} \text{ is specified over } \Gamma_k \end{cases} \\
b^{(mk)} &= \begin{cases} \bar{\phi}_k \left(-F_{2k}(\bar{\mathbf{x}}_m) + \frac{1}{2}\delta^{(mk)}\right), & \text{if } \phi \text{ is specified over } \Gamma_k \\ \bar{p}_k F_{1k}(\bar{\mathbf{x}}_m), & \text{if } \frac{\partial \phi}{\partial n} \text{ is specified over } \Gamma_k \end{cases} \\
\delta^{(mk)} &= \begin{cases} 0\,, m \neq k \\ 1\,, m = k \end{cases} \\
z^{(k)} &= \begin{cases} \bar{p}_k\,, & \text{if } \phi \text{ is specified over } \Gamma_k \\ \bar{\phi}_k\,, & \text{if } \frac{\partial \phi}{\partial n} \text{ is specified over } \Gamma_k \end{cases}
\end{aligned} \tag{11}$$

After solving the above linear system, the values of ϕ and $\frac{\partial \phi}{\partial n}$ will be known over the elements Γ_1, Γ_1, Γ_3, ..., Γ_N and equation (7) with $\lambda(\mathbf{x}_0) = 1$ represents an explicit formula for computing ϕ at the interior of Ω, as follows:

$$\phi(\mathbf{x}_0) \approx \sum_{k=1}^{N} \{\bar{\phi}_k F_{2k}(\mathbf{x}_0) - \bar{p}_k F_{1k}(\mathbf{x}_0)\},\ \forall(\mathbf{x}_0) \in \Omega. \tag{12}$$

Mixed Eulerian-Lagrangian method (MEL)

In order to represent the free surface elevation with distributed nodes on the boundary, the Mixed Eulerian-Lagrangian method (MEL) is employed. The use of the fully nonlinear free surface time-stepping method for 2D waves by the MEL technique was first introduced by Longuet-Higgins and Cokelet, (1976). Here we use the so-called semi-Lagrangian method when a given node moves only in the vertical direction. Then the free surface boundary conditions in equations (2) and (3) is modified as follows:

$$\frac{D\eta}{Dt} = \frac{\partial \phi}{\partial z} + \frac{\partial \phi}{\partial x}\frac{\partial \eta}{\partial x} \qquad \text{on } z = \eta. \tag{13}$$

$$\frac{D\phi}{Dt} = -g\eta - \frac{1}{2}|\nabla\phi|^2 + \frac{D\eta}{Dt}\frac{\partial \phi}{\partial z} \qquad \text{on } z = \eta. \tag{14}$$

Smoothing scheme

During the simulation of nonlinear waves, sawtooth instability may occur on the free surface. To avoid this, we use a Chebyshev 5-point smoothing scheme as introduced by Longuet-Higgins and Cokelet, (1976) along the free surface for every 4^{th} time step:

$$\hat{f}_i = \frac{1}{16}(-f_{i-2} + 4f_{i-1} + 10f_i + 4f_{i+1} - f_{i+2}). \tag{15}$$

Sequence of the Solution Procedure

The sequence followed for computing the BEM solution is as follows:

1. Define the number of elements on wall_1, wall_2, wall_3 and the free surface.
2. Initialize the free surface profile.
3. Specify ϕ or $\frac{\partial\phi}{\partial n}$ on the boundaries.
4. Solve Laplace's equation for $\frac{\partial\phi}{\partial n}$ or ϕ on the boundary.
5. Generate the grid to compute the velocity potential in the interior points.
6. Use finite differences to approximate the velocities at each point in the grid.
7. Approximate $\frac{\partial\eta}{\partial x}$ at each node on the free surface by finite differences.
8. Apply the MEL dynamic and kinematic B.C. given in equations (13) and (14) to update ϕ and η on the free surface points except the first and last nodes.
9. Use the quadratic extrapolation to approximate the ϕ and η for the first two nodes and last two nodes on the free surface.
10. Use (15) to smooth the free surface and ϕ on the free surface except the first and last two nodes.
11. Advance the solution in time by repeating the procedure (step 3-10) at every time step up to the final step.

THE VIRTUAL SOURCE METHOD

Langfeld et al. (2016) presented the virtual source method (VSM) to find the solution to Laplace's equation (1) for the problem expressed in figure 1. They introduced dimensionless variables by chosen the tank width L_x and height L_z as fundamental units of length as:

$$x = L_x\,\bar{x}, \qquad z = L_z\,\bar{z}, \tag{16}$$

while the dimensionless variables of velocity, velocity potential and time is defined as:

$$\begin{aligned} u &= \sqrt{g\,L_z}\tfrac{L_z}{L_x}\bar{u}, \qquad v = \sqrt{g\,L_z}\bar{v} \\ \phi &= \sqrt{g\,L_z^3}\bar{\phi}, \qquad\quad t = \sqrt{L_z/g}\bar{t} \end{aligned} \tag{17}$$

Finally, the kinematic and dynamic boundary conditions of the free surface (3)and (2) becomes, respectively:

$$\frac{\partial\bar{\phi}}{\partial\bar{t}} = -\bar{z} - \frac{1}{2}\,,\left[\kappa^2\bar{u}^2 + \bar{v}^2\right], \qquad \text{on } z = \eta, \tag{18}$$

$$\frac{\partial\bar{h}}{\partial\bar{t}} = -\kappa^2\bar{u}\frac{\partial\bar{h}}{\partial\bar{x}} + \bar{v}(\mathbf{x},t), \qquad \text{on } z = \eta, \tag{19}$$

where $\kappa = \frac{L_z}{L_x}$.

According to Langfeld et al., (2016), the velocity potential can be expressed analytically by the following sum:

$$\phi(\mathbf{x},t) = \sum_{n\in\mathbb{N}} \sigma_n(t)\cos(k_n x)F\left(\kappa n,\ \frac{z}{L_z}\right), \tag{20}$$

where $\sigma_n(t)$ is the n^{th} component of the Fourier cosine transform of the velocity potential along the top boundary, $k_n = \frac{\pi}{L_x}n$ and

$$F(k,\bar{z}) = \sum_{\nu=0}^{\infty}(-1)^{\nu}\left[\mathrm{e}^{-\pi k(2\nu+1+\bar{z})} + \mathrm{e}^{-\pi k(2\nu+1-\bar{z})}\right], \quad k > 0. \tag{21}$$

The function F consists of an alternating sum with rapidly vanishing terms. It can be therefore numerically evaluated in a rapid and reliable way.

Numerical Implementation of the VSM

To compute the velocity potential and free surface components, the infinite sum (20) is replaced by a finite sum with a finite frequency components N_c as:

$$\phi(\mathbf{x},t) \approx \sum_{n=1}^{N_c} \sigma_n(t)\cos(k_n x)F\left(\kappa n,\ \frac{z}{L_z}\right). \tag{22}$$

From the last equation, the velocity components can be found analytically at any point in space and time (mesh-free),

$$\nabla\phi(\mathbf{x},t) \approx \sum_{n=1}^{N_c} \sigma_n(t)\nabla\left[\cos(k_n x)F\left(\kappa n,\ \frac{z}{L_z}\right)\right]. \tag{23}$$

Then,

$$u(\mathbf{x},t) \approx -\sum_{n=1}^{N_c} \sigma_n(t)\,k_n\cos(k_n x)F\left(\kappa n,\ \frac{z}{L_z}\right), \tag{24}$$

$$v(\mathbf{x},t) \approx \sum_{n=1}^{N_c} \sigma_n(t)\,\cos(k_n x)\,\frac{\partial F}{\partial z}\left(\kappa n,\ \frac{z}{L_z}\right). \tag{25}$$

Now, the dimensionless Bernoulli equation (18) can be written as:

$$\frac{\partial\bar{\phi}}{\partial\bar{t}} = -\bar{z} - \frac{1}{2}\,,\left[\kappa^2\bar{u}^2 + \bar{v}^2\right] = B\left(\bar{\mathbf{x}},\eta(\bar{x},\bar{t}),\sigma_n(\bar{t})\right) \qquad \text{on } z = \eta. \tag{26}$$

Hence,

$$\sum_{n=1}^{N_c}\frac{d\sigma_n(\bar{t})}{d\bar{t}}\cos(k_n\bar{x})F\left(\kappa n,\bar{z}\right) = B(\bar{\mathbf{x}},\eta(\bar{\mathbf{x}},\bar{t}),\sigma_n(\bar{t})). \tag{27}$$

In order to calculate $\frac{d\sigma_n(\bar{t})}{d\bar{t}}$, choose a set of resolution points N_x, $N_x > N_c$, then:

$$\sum_{n=1}^{N_c}\frac{d\sigma_n(\bar{t})}{d\bar{t}}\cos(k_n\bar{x}_i)F\left(\kappa n,\bar{z}\right) = B(\bar{\mathbf{x}}_i,\eta(\bar{\mathbf{x}}_i,\bar{t}),\sigma_n(\bar{t})), \quad i = 1,...N_x. \tag{28}$$

The last equation produces an overdetermined linear system to compute the time derivative of $\sigma_n(t)$. In this paper, we used the least squares to solve the above system then we used Runge-Kutta 4 integration to find $\sigma_n(t)$. However, Runge-Kutta integration need to compute the time derivative $d\eta/dt$. Langfeld et al., (2016) used Fourier expansion of the spatial dependence to compute the free surface elevation analytically as:

$$\bar{h}(\bar{x},\bar{t}) = \sum_{k=0}^{N_A}[a_k(\bar{t})\cos(\frac{2\pi}{L_x}k\,\bar{x}) + b_k(\bar{t})\sin(\frac{2\pi}{L_x}k\,\bar{x})], \tag{29}$$

where N_A is the number of frequency components.
The latter equation represent the *Airy mode decomposition* and the spatial derivative is known analytically by:

$$\frac{\partial}{\partial\bar{x}}\bar{z}(\bar{x},\bar{t}) = \sum_{k=0}^{N_A}[-ka_k(\bar{t})\sin(\frac{2\pi}{L_x}k\,\bar{x}) + kb_k(\bar{t})\cos(\frac{2\pi}{L_x}k\,\bar{x})] = A\left(\bar{x},a_k(\bar{t}),b_k(\bar{t})\right). \tag{30}$$

Therefore, from equations (19),(24),(25),(29)and (30) one can get,

$$\sum_{k=0}^{N_A}[\frac{da_k(t)}{dt}\cos(\frac{2\pi}{L_x}k\,x)+\frac{db_k(t)}{dt}\sin(\frac{2\pi}{L_x}k\,x)]=-\kappa^2\,\bar{u}\,A\,(\bar{x},a_k(\bar{t}),b_k(\bar{t}))+\bar{v}$$

$$=H\,(\bar{x},a_k(\bar{t}),b_k(\bar{t}),\sigma_n(t)) \tag{31}$$

In the same manner of computing $d\sigma_n(t)/dt$, choose a set of $N_s \geq 2N_A$ points for $\bar{x}$, then the overdetermined system can be solved again using least squares. The use of Runge-Kutta 4 integration now can give $a(t)$, $b(t)$, and $\sigma_n(t)$ at time t.

Sequence of the Solution Procedure

For VSM, the sequence of solution can be summarised as:

1. Define the tank lengths, number of frequency components N_c and resolution points N_s.
2. Initialize the free surface profile.
3. Define the linear system (28) and solve it by using least squares.
4. Define the linear system (31) and solve it by using least squares.
5. Use Runge-Kutta 4 integration to find $a(t)$, $b(t)$, and $\sigma_n(t)$
6. Advance the solution in time by repeating the procedure (step 3-5) at every time step up to the final step.

COMPUTATION OF ENERGY AND VOLUME

To check the accuracy of NWT models, Grilli et al. (1989) reported that a global check of the time stepping accuracy is provided by the volume error relative to initial volume. This is:

$$Vol\_err=\frac{Vol(t)-Vol_0}{Vol_0}, \tag{32}$$

where Vol_0 is the initial volume of water in the tank and $Vol(t)$ is defined as:

$$Vol(t)=\int_\Gamma h(x,t)\,dx, \tag{33}$$

where Γ is the bottom wall, in dimensionless units the, we obtain:

$$Vol(t)=L_x\,L_y\,\overline{Vol}(\bar{t}) \tag{34}$$

$$\overline{Vol}(\bar{t})=\int\bar{h}(\bar{x},\bar{t})\,d\,\bar{x}. \tag{35}$$

To asses the energy conservation, the total energy defined as the sum of kinetic energy and potential energy. Following Langfeld et al.(2016), the kinetic energy is given by:

$$KE(t)=\frac{1}{2}\rho\int_{FS}\phi(\mathbf{x},t).\nabla\phi(\mathbf{x},t).d\mathbf{s}, \tag{36}$$

where,

$$d\mathbf{s}=\begin{pmatrix}-dh/dx\\1\end{pmatrix}. \tag{37}$$

Thus,

$$KE(t)=\tfrac{1}{2}\rho\int_{FS}\phi(\mathbf{x},t)\left[-u\tfrac{\partial h(x,t)}{\partial x}+v\right]dx$$

$$=\frac{1}{2}\rho\int\phi(\mathbf{x},t)\frac{\partial h(x,t)}{\partial t}dx \tag{38}$$

The dimensionless kinetic energy is defined by:

$$KE(t)=\rho\,g\,L_y^2\,L_x\,\overline{KE}(\bar{t}), \tag{39}$$

where,

$$\overline{KE}(\bar{t})=\frac{1}{2}\int_0^1\bar{\phi}(\bar{x},\bar{t})\frac{\partial\bar{h}(\bar{x},\bar{t})}{\partial\bar{t}}d\,\bar{x}. \tag{40}$$

The potential energy is given by:

$$PE(t)=\frac{1}{2}\rho g\int(h(x,t))^2dx. \tag{41}$$

Dimensionless potential energy is given by:

$$\overline{PE}=\rho\,g\,L_y^2\,L_x\,\overline{PE}(\bar{t}), \tag{42}$$

i.e.

$$\overline{PE}(\bar{t})=\frac{1}{2}\int_0^1\left(\bar{h}(\bar{x},\bar{t})\right)^2d\,\bar{x}. \tag{43}$$

For the BEM the model, the global volume, kinetic energy and potential energy are computed numerically by using the numerical integration of quadrilateral elements as presented in Smith et al. (2014). For the VSM model, the kinetic energy is computed numerically from equation (40) by using Simpson's rule. Global volume and potential energy were found by evaluating equations (35) and (43) analytically as follows:

$$\overline{Vol}(\bar{t})=a_0(\bar{t}), \tag{44}$$

$$\overline{PE}=(a_0(\bar{t}))^2+\frac{1}{2}\sum_{k=1}^{N_A}\left[(a_k(\bar{t}))^2+(b_k(\bar{t}))^2\right] \tag{45}$$

NUMERICAL RESULTS AND DISCUSSION

In this section, the numerical results of both BEM and VSM for a standing wave test problem are discussed through checking the global accuracy by computing the volume and energy.

Standing sinusoidal waves are simulated in a numerical wave tank as shown in figure 1. The dimensions of the tank are $L_x = 1m$ width and $h_0 = 0.1m$ initial water height. The initial fluid configuration is at rest. The wave shape is initially set to:

$$h(x,t)=h_0+a\cos(kx)\cos(\omega t)+\tfrac{k\,a^2}{L_x}[\cos^2(\omega t)$$

$$-\frac{1}{4\cosh^2(kh_0)}+\frac{3}{4\sinh^2(kh_0)}\cos(2\omega t)]\cos(2kx), \tag{46}$$

where, $k=\frac{2\pi}{L_x}$ is the wave number, $\omega=[k\,g\,\tanh(kh_0)]^{1/2}$ is the angular frequency and $T=\frac{2\pi}{\omega}$ is the wave period. For all simulations, N_A and N_s are chosen as $N_A = N_c$ and $N_s = N_x$.

Figures 2 and 3 present the time histories of the relative error of the global volume and total energy for two wave amplitudes $a = 0.01$ and $a = 0.02$ for both BEM and VSM models. For the BEM scheme, we use 250 boundary element along the free surface, 50 on wall_3 and 25 on each wall_1 and wall_2. The VSM scheme is run with 100 resolution points N_x and 15 frequency components N_c. The time step is chosen as

$\Delta t/T = 1/1600$ for both schemes. It can be seen that for VSM scheme, relative errors for both total energy and global volume are close to zero for both large and small amplitude. However, it can be noticed that the volume and energy conservation is affected by the by the wave amplitude value. Moreover, there is a clear loss of energy and volume for high amplitude when the BEM scheme is used.

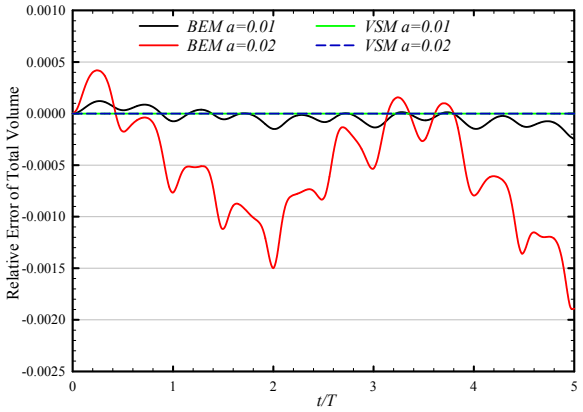

Fig. 2 Relative error of global volume as a function of time

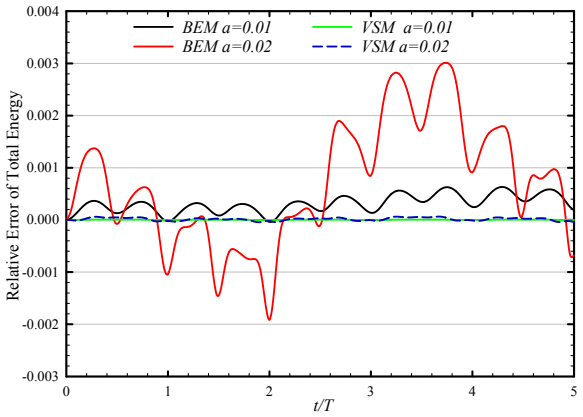

Fig. 3 Relative error of global energy as a function of time.

For more analysis, we define the solution of $\Delta t/T = 1/3200$ and the same numbers of boundary elements above as a reference solution for BEM scheme, while the VSM reference solution is chosen with $\Delta t/T = 1/1600$ and the same numbers of resolution and frequency components as above. In order to determine the approximate order of accuracy of the current BEM and VSM schemes, the l_2-norm of the potential and kinetic energy error compared with the reference solutions are plotted against the numbers of time steps per period for different amplitudes. Generally, it is found that as time step is decreased the l_2-norm error of energy decreases in value.

Figures 4 and 5 show the l_2-norm in the kinetic and potential energy for the reference BEM ad VSM solutions versus the number of time steps per wave period. It can be observed that for both BEM and VSM, the error tends to be small as the wave amplitude value decreases. The results show that the convergence rate to the reference VSM solutions is better than fourth order. However, the convergence rate to the reference BEM solutions is less than second order.

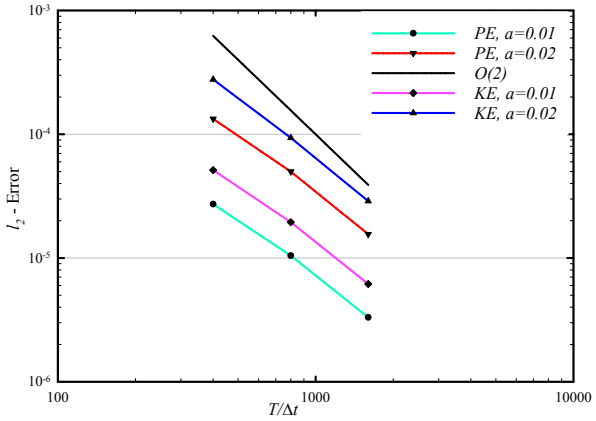

Fig. 4 The (log-log) scale plot of the l_2-norm of errors in the potential and kinetic energy between BEM solutions and reference solution versus the number time steps per period.

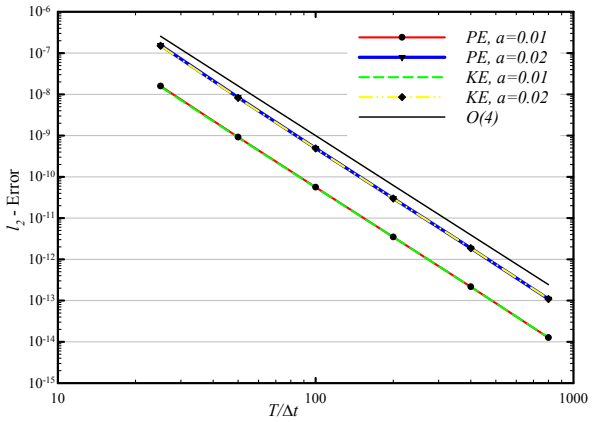

Fig. 5 The (log-log) scale plot of the l_2-norm of errors in the potential and kinetic energy between VSM solutions and reference solution versus the number time steps per period.

For fixed N_x, N_c, and for time step $< T/25$, the results of the VSM simulations showed a fixed error in total energy. In order to indicate the error source, we fixed the time step and ran the simulation with various resolution points N_x and frequency components N_c. The number of frequency components does not affect the solution when N_c is between 15 and 35. However, the results showed that the error increased as the number of frequency components increased above 35 and this possibly due to ill-conditioning of the resulting matrix system.

In order compare computation times, we have measured the computations time of the test problem above when $a = 0.02$ for 5 wave periods. The parameters are chosen as 100 and 200 boundary elements along the free surface for the BEM and the same number of resolution points N_x are chosen for the VSM while the number of frequency component N_C IS chosen as 15 because as we see above there no benefit from increasing N_c. Table 1 shows the simulation computation time for each method. It can be noticed that in both BEM and VSM, the computation time is directly proportional to the time step size as expected. It can be seen that the VSM is cheaper than the BEM in terms of computation time. Moreover, doubling the 'grid size' leads to computation times increasing by a factor of around 8 for BEM but only 2.6 for VSM. We anticipate similar behaviour in three spatial dimensions, making VSM very competitive for such computations.

Table 1 Computation time.

t	BEM			VSM		
	100	200	ratio	100	200	ratio
400	308.2	2640	8.566	161.2	420	2.605
800	628.8	5460	8.683	328.8	840	2.555
1600	1251.2	10448	8.350	656.8	1696	2.582
3200	2601.6	21360	8.210	1336.2	3360	2.515

Figure 6 shows the time history of the relative error in total energy for different numbers of resolution points N_x and for two wave amplitudes. It can be seen that the VSM scheme conserves energy for small amplitudes better than the large amplitude. However, it can also be concluded that the scheme conserves energy more effectively by increasing the number of resolution points.

Note that we used the solution of $\Delta t/T = 1/400$, $N_c = 15$ and $N_x = 640$ as a reference solution in order to test the convergence rate to both analytical and numerical solutions.

Figure 7 presents, for two different amplitudes, the l_2-norm of errors for the total energy as a function of time for both the reference numerical solution and the initial potential energy. It can be seen that the convergence rate to the initial potential energy is up to $O(1/2)$, while the convergence rate to the reference numerical solution is up to the first order which is more rapid than the convergence to the initial potential energy.

To assess the stability of VSM, we run the simulation for 140 wave periods. Figures **??** and **??** presents the relative error in total energy and total volume as functions of time for two different amplitudes and various time steps. It can be seen that the the scheme is of high stability if we use more than 50 time steps per wave cycle. The results showed that the relative error in total volume is small even after a long time of simulation. However, the volume is slightly increases if we use a relatively large step of $T/25$.

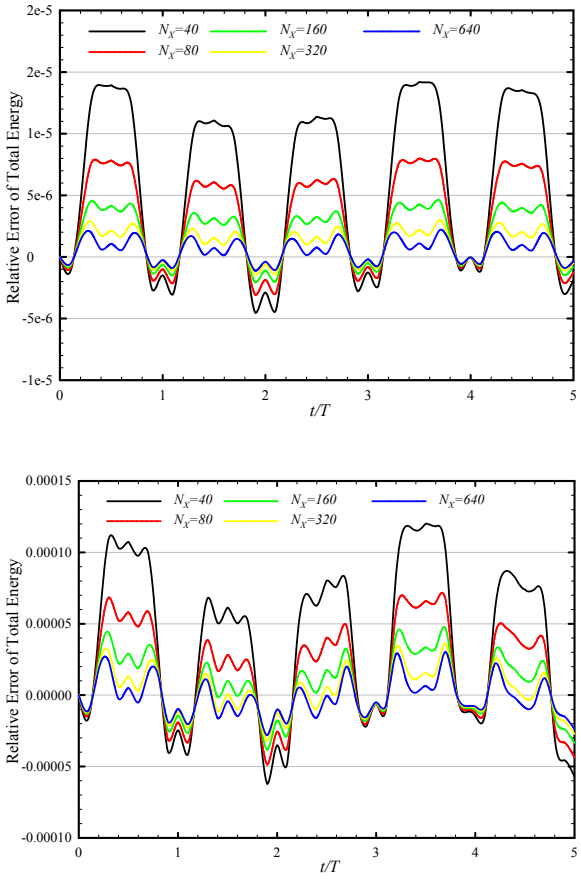

Fig. 6 Time history of total energy relative error for various time resolution points N_x. $a = 0.01$ (top); a=0.02(bottom).

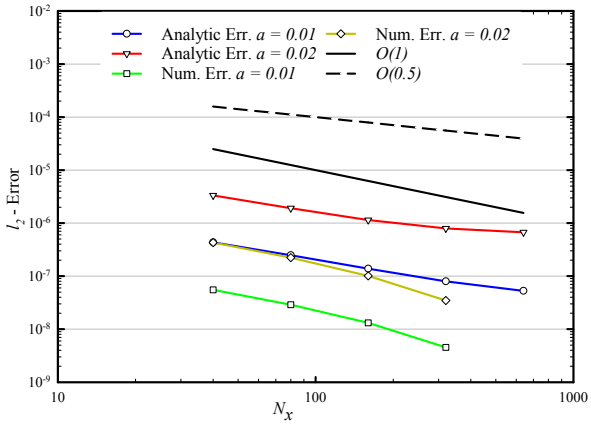

Fig. 7 The (log-log) scale plot of the l_2-norm of errors in the potential and kinetic energy between VSM solutions and reference solution versus theN_x.

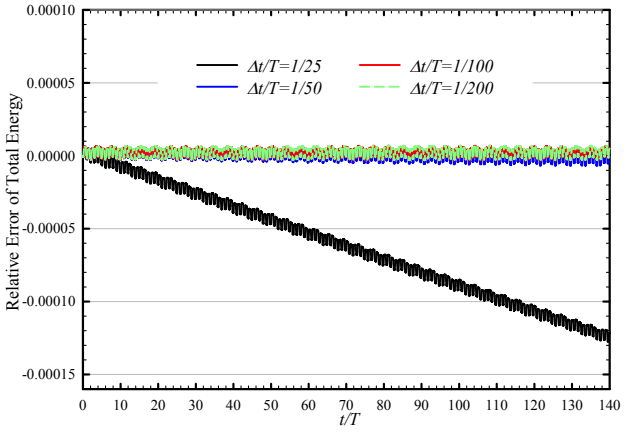

Fig. 8 Time history of total energy relative error for $a = 0.01$ and various time resolution points N_x.

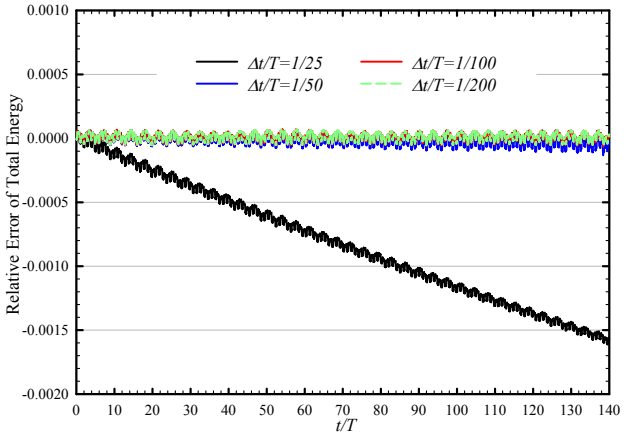

Fig. 9 Time history of total energy relative error for $a = 0.02$ and various time resolution points N_x.

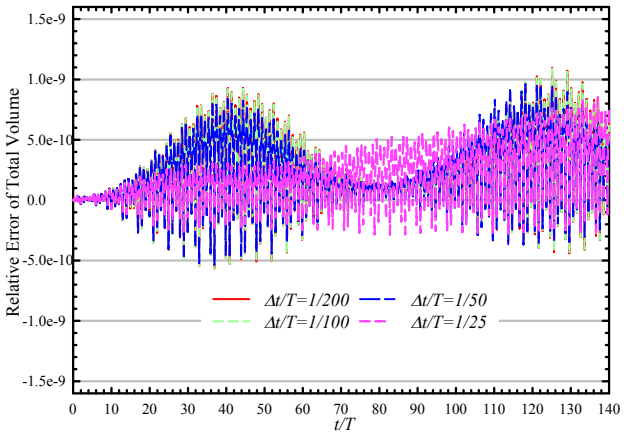

Fig. 10 Time history of total energy relative error for $a = 0.01$ and various time resolution points N_x.

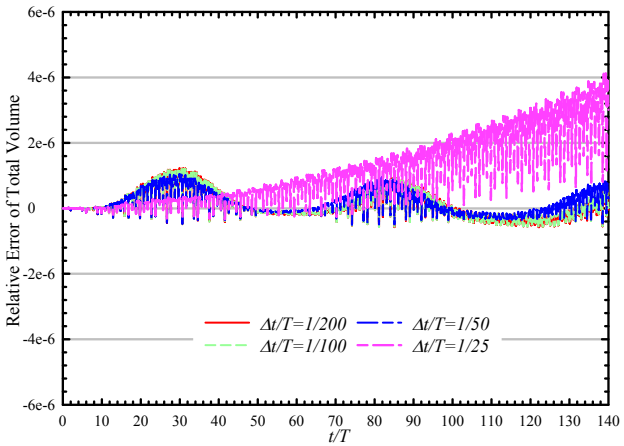

Fig. 11 Time history of total energy relative error for $a = 0.02$ and various time resolution points N_x.

CONCLUSIONS

This work discussed the global accuracy of BEM and VSM schemes for standing wave simulations. We have derived an analytical formulas to compute the potential energy and volume for the VSM scheme. We found that the BEM scheme conserves energy and volume more effectively for small amplitudes whilst there are clear variations in total energy for high amplitudes. The results showed that the VSM is cheaper than the BEM in terms of computation time. Moreover, the ratio of computation times when we double the number of boundary elements and resolution points is about 8 in BEM and 2.5 in VSM which makes the VSM more efficient in high dimensions problems. The VSM has been found to have excellent conservation of volume as the error is close to zero even for high amplitudes. In terms of energy conservation, we have found that the error convergence rate was up to fourth order for both small and large amplitudes. However, the relative errors in the total energy seem to be insensitive to the time step so long as the time step is sufficiently small. This magnitude of errors can be reduced by increasing N_x. The error convergence rate to the best numerical solution is up to first order in N_x, while it converges to the initial potential energy up to order $O(1/2)$. It has been found that the energy conservation is affected if we used a large number of frequency components and that may be due to the ill conditioning of the system matrix. Future work will include the development of virtual source method significantly for progressive waves, wave/structure interactions, and other types of free surface flow problems.

REFERENCES

Huang, CJ, Zhang, EC. and Lee, JF (1998). "Numerical simulation of nonlinear viscous wavefields generated by piston-type wavemaker", Journal of Engineering Mechanics , 124(10), 1110-1120.

Grilli, ST, Skourup, J. and Svendsen, IA (1989). "An Efficient Boundary Element Method for Nonlinear Water Waves", Engineering Analysis with Boundary Elements, 6(2), 97-107.

Grilli, S, T, Guyenne, P, and Dias, F, (2001). "A fully non-linear model for threedimensional overturning waves over an arbitrary bottom", International Journal for Numerical Methods in Fluids 35(7), 829867. Smith, I, Griffiths, D, and Margetts, L (2014). "Programming the Finite Element Method," Wiley, 2014.

Langfeld, K, Graham, DI, Greaves, DM, Mehmood, A, Reis, T, (2016). "The Virtual Source Approach to Non-Linear Potential Flow Simulation," Proc 26th Int Offshore and Polar Eng Conf, Rhodes, Greece, 26 June-2 July, 2016.

Longuet-Higgins, M, and Cokelet, E (1976). "The Deformation of Steep Surface Waves on Water. I. A Numerical Method of Computation," Proceedings of the Royal Society of London. Series A, Mathematical and Physical Sciences, 350(1660), 1-26.

Park, JC, Uno, Y, Matsuo, H, (2001). "Reproduction of Fully-Nonlinear Multi-Directional Waves by a 3D Viscous Numerical Wave Tank," Proc 11th Int Offshore and Polar Eng Conf, Stavanger, Norway,17-22 June, 2001.

Smith, I, Griffiths, D, and Margetts, L (2014). "Programming the Finite Element Method," Wiley, 2014.

Wu, G, and Taylor, R, E, (1994). "Finite element analysis of two-dimensional non-linear transient water waves", Applied Ocean Research 16(6), 363372.